

Article

A Facile Synthesis of Flower-like Iron Oxide Nanoparticles and Its Efficacy Measurements for Antibacterial, Cytotoxicity and Antioxidant Activity

Nazish Tabassum ¹, Virendra Singh ², Vivek K. Chaturvedi ³, Emanuel Vamanu ^{4,*} and Mohan P. Singh ^{1,*}¹ Centre of Biotechnology, University of Allahabad, Prayagraj 211002, India² Centre for Interdisciplinary Research in Basics Sciences, Jamia Millia Islamia, New Delhi 110025, India³ Department of Gastroenterology, Institute of Medical Sciences, Banaras Hindu University, Varanasi 221005, India; vkchaturvedi.nbt@gmail.com⁴ Faculty of Biotechnology, University of Agricultural Sciences and Veterinary Medicine of Bucharest, 011464 Bucharest, Romania

* Correspondence: email@emanuelvamanu.ro (E.V.); mpsingh.16@gmail.com (M.P.S.)

Abstract: The objective of this study was to investigate the rhombohedral-structured, flower-like iron oxide (Fe₂O₃) nanoparticles that were produced using a cost-effective and environmentally friendly coprecipitation process. The structural and morphological characteristics of the synthesized Fe₂O₃ nanoparticles were analyzed using XRD, UV-Vis, FTIR, SEM, EDX, TEM, and HR-TEM techniques. Furthermore, the cytotoxic effects of Fe₂O₃ nanoparticles on MCF-7 and HEK-293 cells were evaluated using in vitro cell viability assays, while the antibacterial activity of the nanoparticles against Gram-positive and Gram-negative bacteria (*Staphylococcus aureus*, *Escherichia coli*, and *Klebsiella pneumoniae*) was also tested. The results of our study demonstrated the potential cytotoxic activity of Fe₂O₃ nanoparticles toward MCF-7 and HEK-293 cell lines. The antioxidant potential of Fe₂O₃ nanoparticles was evidenced by the 1,1-diphenyl-2-picrylhydrazine (DPPH) and nitric oxide (NO) free radical scavenging assays. In addition, we suggested that Fe₂O₃ nanoparticles could be used in various antibacterial applications to prevent the spread of different bacterial strains. Based on these findings, we concluded that Fe₂O₃ nanoparticles have great potential for use in pharmaceutical and biological applications. The effective biocatalytic activity of Fe₂O₃ nanoparticles recommends its use as one of the best drug treatments for future views against cancer cells, and it is, therefore, recommended for both in vitro and in vivo in the biomedical field.

Keywords: Fe₂O₃ nanoparticles; co-precipitation; cancer cell line; cytotoxicity; antibacterial; antioxidant



Citation: Tabassum, N.; Singh, V.; Chaturvedi, V.K.; Vamanu, E.; Singh, M.P. A Facile Synthesis of Flower-like Iron Oxide Nanoparticles and Its Efficacy Measurements for Antibacterial, Cytotoxicity and Antioxidant Activity. *Pharmaceutics* **2023**, *15*, 1726. <https://doi.org/10.3390/pharmaceutics15061726>

Academic Editor: Tania Limongi

Received: 5 May 2023

Revised: 11 June 2023

Accepted: 12 June 2023

Published: 14 June 2023



Copyright: © 2023 by the authors. Licensee MDPI, Basel, Switzerland. This article is an open access article distributed under the terms and conditions of the Creative Commons Attribution (CC BY) license (<https://creativecommons.org/licenses/by/4.0/>).

1. Introduction

Nanotechnology became a game-changing field in technology development in recent years. Among the various nanomaterials, nanoparticles received significant attention due to their unique physical and chemical properties, such as low melting point, specific magnetization, higher surface area, and specific optical properties [1]. These size-dependent properties and minimal harmful effects make them superior and suitable candidates in different areas of human activities [2]. Nanobiotechnology is currently gaining cumulative importance in the fields of nanomedicine, drug delivery, and immunology. Many new promising techniques and methods for synthesizing nanoparticles are being developed through chemical modification, biological reduction, and scaffolding to expand the application of nanobiotechnology in the biomedical field [3,4]. In recent years, various nanomaterials were synthesized by chemical and green synthesis methods. Some researchers used green chemical approaches for the synthesis of metallic nanoparticles. Ullah et al. reported the green synthesis of silver oxide (Ag₂O) nanoparticles using leaves extract of *Parietaria alsinaefolia* as a reducing agent. Furthermore, various biological application was

carried out to evaluate the efficiency of these nanoparticles [5]. In another study, researchers successfully synthesized a composite of silver-graphene nanoparticles ((Ag)_{1-x}(GNPs)_x) via ex situ approach. The composite nanoparticles showed strong anticancer and antifungal properties [6]. Haris and their co-workers synthesized iron oxide nanoparticles from *Oscillatoria limnetica* extract and investigated the biomedical potential of these nanoparticles [7]. Among these nanomaterials, iron oxide nanoparticles (IONPs) catch an attraction by the scientific communities for their unique magnetic properties [8]. Due to their low toxicity and good biocompatibility, IONPs are considered to be the most favorable candidate for bioengineering and biomedical application such as bioimaging, targeted drug delivery, magnetic fluid hyperthermia (MFH), theranostics, detection of biological entities, biosensors, and photoablation therapy [9,10]. For various fundamental and biomedical uses, recent years saw a systematic study of various polymorphs of magnetic NPs such as Fe₃O₄, α-Fe₂O₃, γ-Fe₂O₃, and FeO [11–13]. Among them, hematite (α-Fe₂O₃) is more stable with optical, magnetic, and anticorrosive properties as well as outstanding chemical stability and biocompatibility which is beneficial in different technological applications [14]. These properties of hematite are used in innovative nanomaterial applications such as water splitting, water purification, gas sensing, solar energy conversion, catalyst, and anticorrosive agents [15]. Due to their attractive features, such as good stability, biocompatibility, low cost, and non-toxicity, these nano-sized Fe₂O₃ nanomaterials are more suitable for biomedical applications [16].

Many studies on the synthesis of Fe₂O₃ nanoparticles were conducted in recent years, detailing efficient synthesis methods for size control, stability, biocompatibility, and monodispersed iron oxide nanoparticles [17–19]. Among them, the coprecipitation process, one of the most popular techniques, was frequently used to synthesize Fe₂O₃ nanoparticles. Coprecipitation is a straightforward, affordable procedure that is carried out in comfortable settings without the use of any hazardous solvents [20]. The synthesis process is dependent on several variables, including pH, temperature, the type of salts used, and ionic strength, to produce nanoparticles that are the ideal size and form [21–23].

After knowing about the significance of Fe₂O₃ nanoparticles in biomedical areas, the current research was carried out to synthesize the nanoparticles using a practical co-precipitation approach. Then, using a variety of characterization, physicochemical screening of the produced nanoparticles was performed. Regarding this, human breast cancer (MCF-7) and human embryonic kidney (HEK-293) cell lines were used in the cytotoxic assessment of Fe₂O₃ nanoparticles. Additionally, the effectiveness of Fe₂O₃ nanoparticles against three different bacteria species—*Staphylococcus aureus* (*S. aureus*), *Klebsiella pneumoniae* (*K. pneumoniae*), and *Escherichia coli* (*E. coli*)—was evaluated. The antibacterial ability of human pathogenic bacteria, and cytotoxicity effects against cancer cell lines, suggest the potential of Fe₂O₃ nanoparticles for biomedical applications.

2. Materials and Methods

2.1. Chemicals and Reagents

We bought ammonia solution (25%) and ferrous sulphate heptahydrate (FeSO₄·7H₂O) from Sisco Research Laboratories (SRL) Pvt. Ltd. in India. The following items were acquired from Sigma-Aldrich, India: i.e., dimethyl sulfoxide (DMSO), antibiotics, Dulbecco's Modified Eagle's Medium (DMEM), foetal bovine serum (FBS), trypsin/EDTA, Dulbecco's phosphate-buffered saline (DPBS), and 3-(4,5-dimethylthiazol-2-yl)-2,5-diphenyltetrazolium Sodium nitroprusside. 1, 1-diphenyl, 2-picryl hydrazyl (DPPH) was purchased from Invitrogen in India. Double distilled water (DI) was used in the studies as a standard solvent and for washing.

2.2. Synthesis of Fe₂O₃ Nanoparticles

Fe₂O₃ nanoparticles were synthesized from a simple low-cost coprecipitation route. Then, 0.1 M FeSO₄·7H₂O was dissolved in 50 mL DI water and stirred on a magnetic stirrer vigorously for 45 min. After that, the ammonia solution was added drop by drop

under continuous stirring until the pH reached ~ 12 and the green color precipitate was formed. The solution was placed on magnetic stirring for 1–2 h. Afterward, the solution was removed from the magnetic stirrer until it settled down. The precipitate was washed thoroughly with DI water 2–3 times and dried at 65°C for 5 h and calcinated at 800°C for 3 h [20,24]. The synthesis process of Fe_2O_3 nanoparticles is represented in Figure 1.

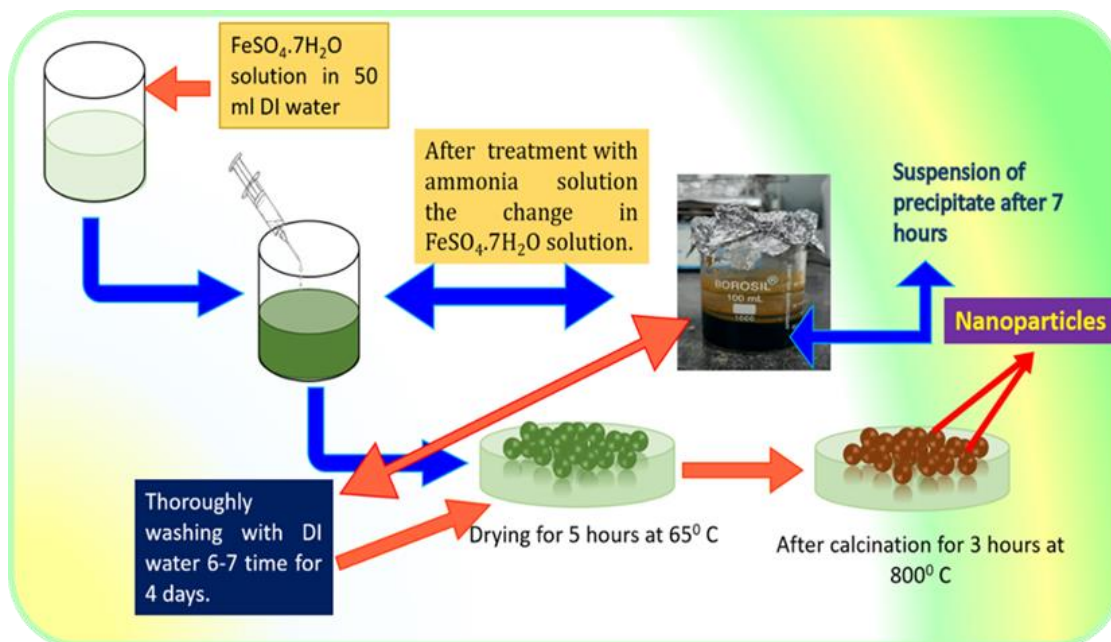


Figure 1. Fe_2O_3 nanoparticles are an emerging player in biomedical applications. Among various synthetic methods, the co-precipitation method appears to be the most successful method for batch production of Fe_2O_3 nanoparticles. The present diagrammatic illustration represents the facile and low-cost synthesis of Fe_2O_3 nanoparticles by modifying the coprecipitation route for better control of particle size.

2.3. Instrumentation

UV-visible spectrophotometer (SPECORD 210 PLUS double beam spectrophotometer, Analytic Jena, Germany) was used at room temperature, and the absorption band of the synthesized sample was measured with a resolution of 1 nm. The manufactured powder sample's phase composition and degree of crystallinity were examined using an XRD diffractometer (Bruker AXSD8) and Cu-K radiation ($\lambda = 1.5406$). The sample's FTIR spectra were captured using a Perkin-Elmer 1600 Fourier transform instrument in the KBr pellet mode between 500 and 4000 cm^{-1} . The morphology and chemistry of nanoparticles were studied using a field emission scanning electron microscopy (FESEM) FEI Quanta 200 F SEM, FEI Company Netherlands instrument with an EDX detector. Transmission electron microscopy with high resolution (HRTEM) (FEI Tecnai TF20) was used for TEM and selected area electron diffraction (SAED) analysis.

2.4. Evaluation of the Cytotoxic Activity of Fe_2O_3 Nanoparticles

2.4.1. Cell Culture

Both the human embryonic kidney (HEK-293) and human breast cancer (MCF-7) cell lines were obtained from the NCCS in Pune, India, and were subcultured in a lab. The cell lines were grown in DMEM, a high glucose medium, which also contained 10% FBS and 2% penicillin/streptomycin. The culture was kept in an incubator with 5% CO_2 at a temperature of 37°C .

2.4.2. MTT Assay

The 3-(4,5-dimethylthiazol-2-yl)-2,5-diphenyltetrazolium bromide (MTT) assay was performed with the Mosdam approach [25]. The culture media were supplemented with the diluted stock solution of Fe₂O₃ nanoparticles. Two distinct 96-well culture plates were seeded with 1×10^5 MCF-7 and HEK-293 cell lines per well and incubated at 37 °C overnight. The cells were treated with various doses of Fe₂O₃ nanoparticles (25, 50, 75, 100, and 125 µg/mL) the next day and were incubated for 24 h at 37 °C with 5% CO₂. The cells that were not exposed served as a control. MTT solution (10 µL) was added to each well after 24 h, and the culture plates were then incubated at 37 °C for 3–4 h. Formazan crystals were dissolved in 100 mL of DMSO following incubation and a reading at 570 nm of the absorbance was taken. The experiment was performed three times, the cell viability percentage was determined using the following formula, and the mean average value was obtained from triplicates.

$$\text{cell viability (\%)} = \frac{(\text{Absorbance of treated cells})}{(\text{Absorbance of control cells})} \times 100$$

2.5. Antibacterial Activity of Fe₂O₃ Nanoparticles

The antibacterial study of the Fe₂O₃ nanoparticles was executed against three different pathogenic bacteria *E. coli* (ATCC-25922), *K. pneumoniae* (ATCC-31488), and *S. aureus* (ATCC-25323) by the disc diffusion method using Kasithevar et al. procedure with some modification [26]. These bacteria were cultured for 24 h in nutrient broth. Afterward, 100 µL (106 CFU/mL) of the bacterial strains was placed on the agar plates to make the culture turf. The Fe₂O₃ nanoparticles were mixed in DMSO to make a stock solution of 1 mg/mL. Later on, 10, 20, 30, and 40 µg/mL of sample disc of nanoparticle were placed on a nutrient agar media plate along with the control (DMSO). The plates were placed in the incubator for 24 h and the respective inhibition zone (mm) for bacterial species were measured. The experiment was performed in triplicates.

2.6. Antioxidant Activity of Fe₂O₃ Nanoparticles

The free radical scavenging activity of the Fe₂O₃ nanoparticles was carried by using 1,1-diphenyl-2-picryl hydrazyl (DPPH) assay. Kurechi and their co-worker's method was followed with minor modifications [27]. Briefly, a stock solution of 2 mg/mL of the Fe₂O₃ nanoparticles and standard solutions of L ascorbate was prepared and diluted to obtain desired concentrations. After that, an equal amount of the diluted solutions and DPPH (0.05 mg/mL) solution was mixed and incubated for 30 min. The experiments were conducted at room temperature. The absorbance was recorded at 517 nm using a spectrophotometer. The scavenging activity was calculated as

$$\text{Scavenging (\%)} = \frac{A_c - A_s}{A_c} \times 100;$$

where A_c -absorbance of the control sample (DPPH) and A_s -absorbance of a sample with DPPH. The experiment was executed in triplicates. Additionally, 0.1 mM DPPH and L-ascorbate were used as a control and standard solution.

The Griess reaction was used to measure the nitric oxide scavenging activity. After oxygen interacts with sodium nitroprusside in a solution at a physiological pH, nitric oxide is produced. Then, 5 mM sodium nitroprusside was mixed with 3 mL of various concentrations of Fe₂O₃ nanoparticles and standard solution L ascorbate in phosphate buffer (pH 7.4) to conduct the nitric oxide assay. Additionally, the solution mixture was left to stand for 30 to 40 min. Then, 1.5 mL of the incubated solution and Griess reagent were combined after the incubation period and left to stand for 30–35 min. A spectrophotometer was used to measure the mixture's absorbance at 540 nm. Using the absorbance values of the mixture in comparison to the control solution, an estimate of the percentage of Fe₂O₃ nanoparticles' nitric oxide scavenging activity was made.

2.7. Statistical Analysis

The one-way ANOVA statistical analysis was carried out with the help of the software Graph Pad Prism v5.0 (San Diego, CA, USA). The differences were deemed significant at $p < 0.05$. Mean \pm standard deviation (mean \pm S.D.) is used to represent all of the data.

3. Results and Discussion

There are two well-known crystalline of Fe_2O_3 : maghemite (the γ -phase) with a cubic structure and hematite (the α -phase) with a rhombohedral structure. According to studies, the phase transformation occurs during calcination at a higher temperature (800 °C) that results in the transformation of α - Fe_2O_3 powder which underwent crystalline structure from an amorphous state [28]. Furthermore, we examined the synthesized Fe_2O_3 nanoparticles by different characterization techniques to obtain information on their physical and chemical properties.

3.1. Physicochemical Characterization of Fe_2O_3 Nanoparticles

The synthesized sample's UV-vis absorption spectrum was measured between 200 and 800 nm, and the related recorded data are presented in Figure 2. The peak at 558 nm in the visible region was attributed to the $6A_1+6A_1-4T_1(4G)+4T_1(4G)$ double excitation process of Fe^{3+} , while the absorption band between 272 and 321 nm was due to the ligand-metal charge transfer transition (direct transition) and assigned to the $6A_1-4T_1(4P)$ and $6A_1-4T_2$ [29]. The twofold excitation process that gives hematite its red color causes the greatest absorption band to be visible at 558 nm [30].

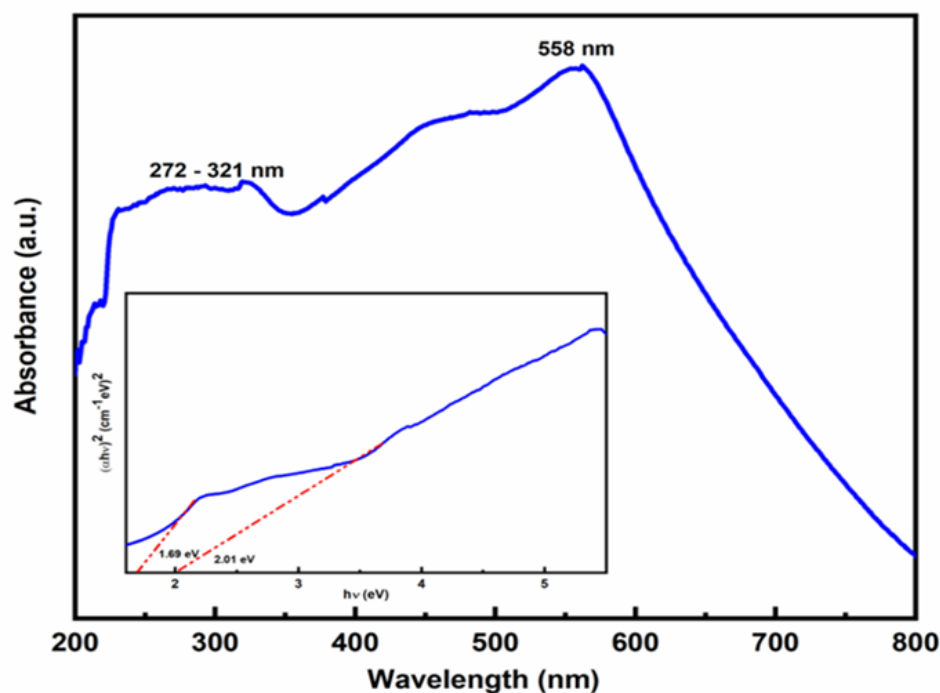


Figure 2. UV-vis absorption spectrum of Fe_2O_3 nanoparticles showing a conformational peak at 558 nm. The inset shows the plot of $(\alpha h\nu)^2$ vs. photon energy ($h\nu$) 1.69 eV and 2.01 eV due to the direct and indirect transition.

The bandgap energy (E_g) of Fe_2O_3 nanoparticles was calculated using Tauc's plot method by the formula

$$\alpha = c(h\nu - E_{bulk})^{1/2}h\nu,$$

where α = absorption coefficient, c = constant, $h\nu$ = photon energy, and E_{bulk} = bulk bandgap. Scientists reported that Fe_2O_3 has an indirect bandgap as well as a direct bandgap [31].

The reported values of the indirect and direct bandgap lie between 1.38–2.09 eV [32] and 1.95–2.35 eV [33,34]. Here, the Fe₂O₃ nanoparticles' bandgap energies were measured to be 1.69 and 2.01 eV, respectively. The energy of a photon is referred to as direct bandgap energy if the momentum of liberated holes in the valence band and electrons in the conduction band is the same. A photon cannot be released during the transition if an electron passes through an intermediate state, which is referred to as indirect bandgap energy. The quantum size effects of the nano-crystallites are responsible for the direct bandgap's presence [35].

The XRD spectrum of the prepared sample shown in Figure 3a denotes the crystallinity and the phase purity. The typical diffraction peaks were observed and matched by the JCPDS data (file no. 00-001-1053), confirming the synthesis of Fe₂O₃ nanoparticles. The sharp peaks at 24.14°, 33.16°, 35.66°, 40.9°, 49.48°, 54.08°, 57.56°, 62.46°, 64.04°, 72.04°, and 75.46° were associated with the plane (012), (104), (110), (113), (024), (116), (122), (214), (300), (1010), and (217), respectively, with a rhombohedral structure. The average crystalline size (*D*) of Fe₂O₃ was calculated by Debye–Scherrer's equation [36], $D = \frac{k\lambda}{\beta \cos \theta}$ where *k* = shape factor (0.89), λ = wavelength of Cu-K α radiation (0.15406 nm), β = full width at half maximum (FWHM), θ = Bragg's diffraction angle. From Scherer's equation, the average size of the Fe₂O₃ nanoparticles is ~24.66 nm.

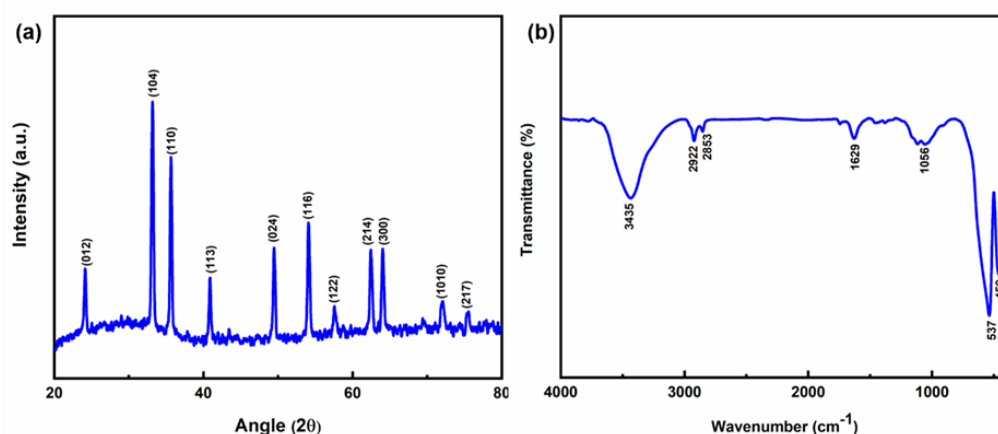


Figure 3. (a) The intense and sharp peaks in the XRD pattern of Fe₂O₃ nanoparticles show the phase purity of synthesized Fe₂O₃ nanoparticles. (b) FTIR spectra of Fe₂O₃ nanoparticles within the wavelength of 4000–400 cm⁻¹.

Figure 3b shows how FTIR was used to investigate the infrared characteristics of synthetic material in the wavelength range (4000–400 cm⁻¹). Peaks associated with metal oxide bonds can be found in the fingerprint range between 1000 and 400 cm⁻¹, whereas water molecule bending and stretching vibrations were responsible for peaks in the region between 400 and 1000 cm⁻¹. The stretching vibration of the water molecules was what caused the absorption peak at 3435 cm⁻¹ to be assigned [37]. The -OH stretching vibration was responsible for the peaks at 2922 and 2853 cm⁻¹. Due to the bending vibration of the crystalline Fe-O bond and the absorbed moisture content, respectively, the peaks at 1629 and 1056 cm⁻¹ were assigned [38]. The 537 and 459 cm⁻¹ peaks were due to the vibration of Fe-O-Fe confirming the presence of Fe₂O₃ [39].

3.2. Morphology and Elemental Mapping of Fe₂O₃ Nanoparticles

Figure 4 depicts the shape of Fe₂O₃ nanoparticles that were studied using FESEM. The flower-like structure of Fe₂O₃ nanoparticles was visible in FESEM pictures (Figure 4a). According to FESEM pictures (Figure 4b), the nanostructures were about 23.4 nm in size, which was in agreement with the X-ray diffraction finding. Additionally, the components

present in the Fe_2O_3 nanoparticles were confirmed by an EDX analysis, as shown in Figure 4c. The presence of the distinct peaks indicates the presence of Fe and O in the nanoparticles. Additionally, the purity of Fe_2O_3 nanoparticles was demonstrated by the peak of Fe and O devoid of any unknown signals. The distribution of components within Fe_2O_3 nanoparticles is depicted in Figure 4d.

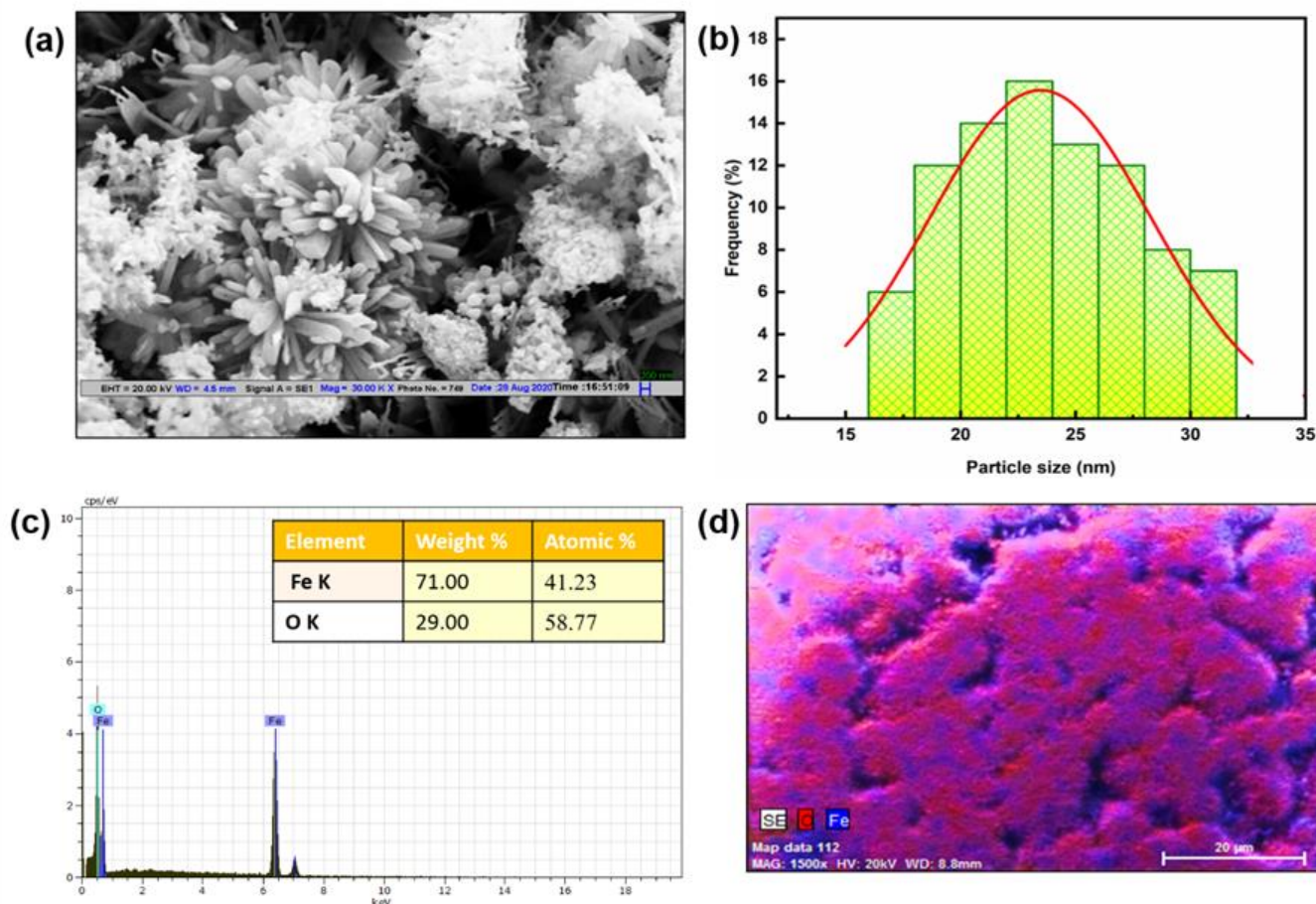


Figure 4. (a) FESEM image of Fe_2O_3 nanoparticles at 200 nm showing the flower-like morphology. (b) The histogram plot for the particle size distribution shows the size of Fe_2O_3 nanoparticles ~ 23.4 nm. (c) EDX spectrum shows the peaks of Fe and O atoms in nanoparticles. (d) Elemental mapping at 20 μm illustrated the distribution of present atoms in Fe_2O_3 nanoparticles.

TEM images of Fe_2O_3 nanoparticles are shown in Figure 5. Due to the agglomeration, the size of the nanoparticles was seen as bigger. With the help of the Image J software, the calculated size of the Fe_2O_3 nanoparticles came out to be 22–45.5 nm (Figure 5a). The bright spot in the SAED pattern demonstrated the crystalline nature of Fe_2O_3 nanoparticles with different orientations (110), and (1010), respectively (Figure 5b). The growth direction of the Fe_2O_3 was parallel to the lattice fringes and the d-spacing of the (012) plane was about 0.354 nm, which was close to the lattice spacing of the rhombohedral Fe_2O_3 (Figure 5c). Considering our XRD study and close observation of the SAED images, it can be concluded that the diffraction rings indicate the rhombohedral Fe_2O_3 structure.

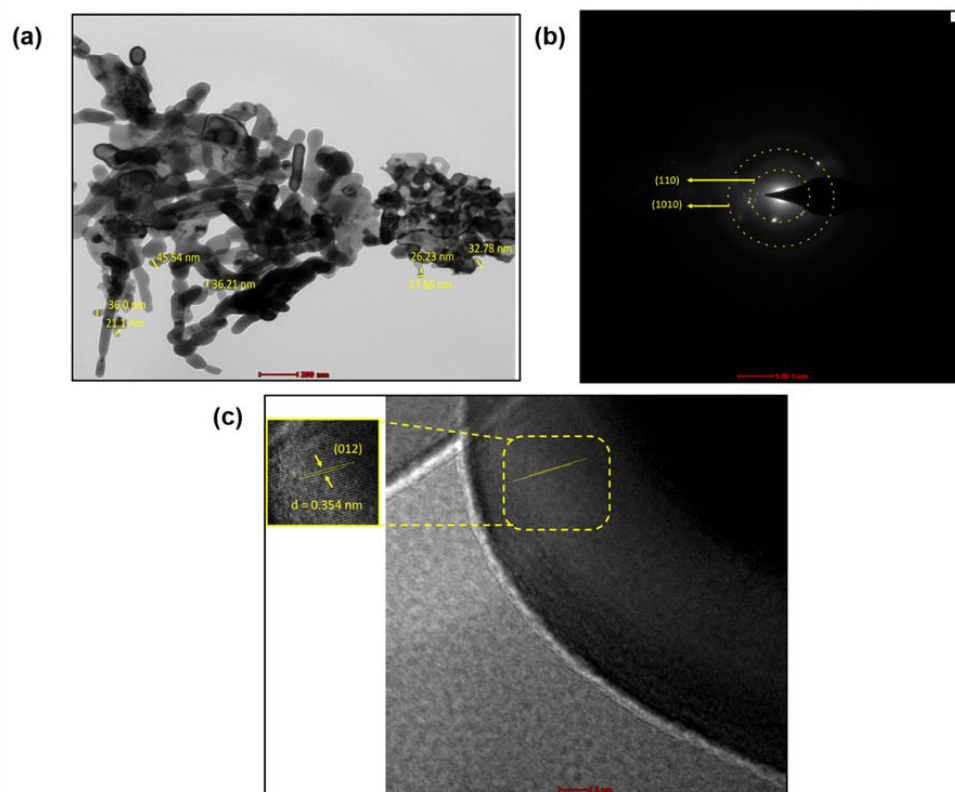


Figure 5. (a) HRTEM micrograph of Fe_2O_3 nanoparticles at 200 nm shows the size of nanoparticles between 22–45.5 nm (b) SAED pattern at 5 nm SAED pattern of Fe_2O_3 nanoparticles indicates crystallinity with different orientation (c) HRTEM image of Fe_2O_3 nanoparticles at 5 nm indicates high crystallinity and shows lattice fringes.

3.3. *In Vitro* Cytotoxicity Assay of Fe_2O_3 Nanoparticles

The MTT test was used to investigate the metabolic effects of Fe_2O_3 nanoparticles on the MCF-7 and HEK-293 cell lines. The relevant answers demonstrated a percentage of cell viability after exposure to Fe_2O_3 nanoparticles at concentrations between 25 and 125 $\mu\text{g}/\text{mL}$ for 24 h (Figure 6). In the MCF-7 cell line, cell viability was reduced to 50% when Fe_2O_3 nanoparticles were present at a concentration of 125 $\mu\text{g}/\text{mL}$ (Figure 6a). The cytotoxicity of Fe_2O_3 nanoparticles against cancer cell lines supported the notion that nanoparticle cytotoxicity is dose-dependent. The normal embryonic kidney cell line (HEK-293) was also subjected to the MTT assay for 24 h, with results revealing less toxicity when compared to the breast cancer cell line (Figure 6b). The potential of Fe_2O_3 nanoparticles was demonstrated by the falling vitality of the cancer cell line in comparison to the normal cell line. Nanoparticles were reported to induce cytotoxic effects on human cells by employing multiple cell-mechanical approaches: (i) through the uptake of free nanoparticles causing defective DNA replication, (ii) through the generation of free radicals and reactive oxygen species (ROS), and (iii) by stressing the cell membrane, the structure of the entire cell membrane is deformed, followed by cell damage or cell death [40,41]. After ROS generation, altered mitochondrial membranes trigger caspase 3, a protein involved in organelle breakdown and DNA fragmentation, which, in turn, triggers apoptosis and cell cycle arrest. Apoptosis initiation leads to the activation of cell-signaling pathways, including activation of p53 protein, and increased p53 protein leads to cell death and nuclear destruction [42]. Moreover, the apoptosis pathways and method for cell death still need to be explained, through *in vitro* and *in vivo* studies.

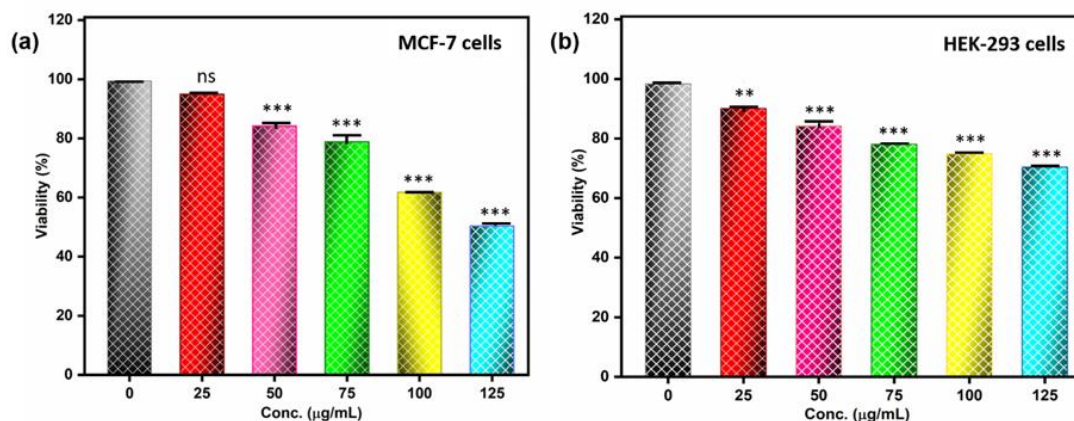


Figure 6. (a) Cell viability assay of Fe_2O_3 nanoparticles at different concentrations illustrated the dose-dependent cytotoxicity against the cancer cell line (MCF-7). (b) Cell viability assay against normal cell line (HEK-293) shows less toxicity as compared to cancer cell line. The graph representation showing the significant activity ($p < 0.05$ was considered to be statistically significant. The symbols **, *** represents, $p < 0.01$, $p < 0.001$).

Previously, researchers illustrated the cytotoxicity of Fe_2O_3 nanoparticles and nanocomposite of $\alpha\text{-Fe}_2\text{O}_3/\text{Co}_3\text{O}_4$ on MCF-7 cell line for 24 h, showing that the nanocomposites are more toxic than $\alpha\text{-Fe}_2\text{O}_3$ [43]. In another study, the cytotoxic efficiency on the A549 cell line was performed for 24 h and showed 50% cell viability at 970 $\mu\text{g}/\text{mL}$ concentration [44]. However, our results showed that at 125 $\mu\text{g}/\text{mL}$ concentration, 50% MCF-7 cell line were viable, indicating good cytotoxic activity of Fe_2O_3 nanoparticles. Based on the result, we can say that Fe_2O_3 nanoparticles can be used as a cytotoxic agent in cancer cell line.

3.4. In Vitro Antibacterial Assessment of Fe_2O_3 Nanoparticles

The antibacterial action of synthesized Fe_2O_3 nanoparticles was conducted upon pathogenic bacteria, namely *S. aureus*, *E. coli*, and *K. pneumoniae*, employing the disc diffusion method. The inhibition zone showed the antibacterial activity of the Fe_2O_3 nanoparticles. The Fe_2O_3 nanoparticles revealed good inhibitory potential on bacterial pathogens (Figure 7). The probable mechanisms of bacterial cell death induced by the Fenton reaction were as reported in the literature [45]. After exposure to Fe_2O_3 nanoparticles to the pathogens, the iron ions released from nanoparticles can cross the membrane either through active uptake into cells or through leakage from sites of reduced membrane integrity. Highly reactive hydroxyl radicals formed when Fe^{2+} reacts with hydrogen peroxide primarily cause oxidative damage. Fe^{3+} can be reduced by NADH to regenerate Fe^{2+} . OH radicals can also damage DNA, proteins, and lipids. Fe^{2+} can also directly damage DNA, resulting in cell death of pathogens [46].

Among three pathogenic bacteria, *E. coli* showed more activity than other bacteria. It was also shown that after increasing the dose of Fe_2O_3 nanoparticles, the inhibition zone increased, as shown in Figure 8 and Table 1. The observations reported that a smaller amount of Fe_2O_3 nanoparticles are sufficient for the activity against the tested bacterial strains. Our results are comparable with the results reported by Saquib and their co-workers [19].

Researchers discovered that ROS causes oxidative stress, which is why antibacterial medications exhibit bactericidal characteristics [47]. Additionally, several studies showed that ROS is crucial for cell signalling and death [48]. Due to the production of ROS, one of the most well-known silver nanoparticles exhibits antibacterial potential [49]. In our material, it was expected that Fe_2O_3 nanoparticles, which prevent microbial development, can produce ROS (Figure 9). The process by which hydrogen peroxide (H_2O_2) was produced when iron (Fe^{2+}) and oxygen interacted was described by Keenan et al. [50]. Additionally, this H_2O_2 interacted with Fe^{2+} ions to create hydroxyl (OH^{\cdot}) radicals, which damage

macromolecules and membranes. Numerous studies showed that nanoparticles of various sizes can enter cells, interact with intracellular oxygen, and cause oxidative stress, which weakens the membrane [46,51,52]. Additionally, according to several studies, the concentration of nanoparticles was a crucial element in boosting antibacterial activity [53,54].

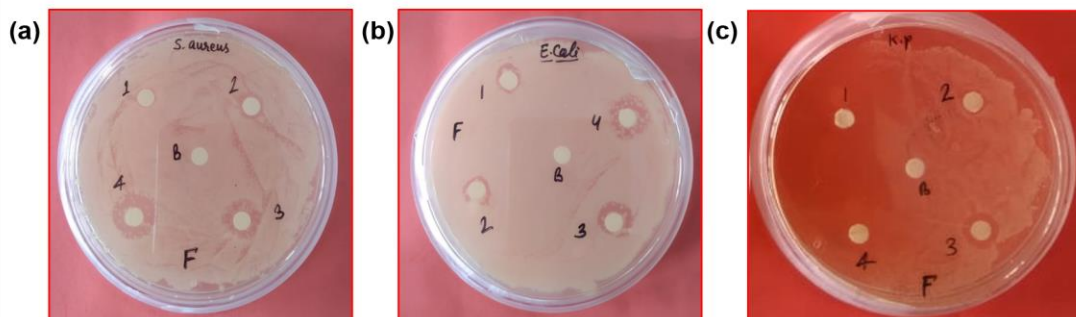


Figure 7. Antibacterial activity of Fe₂O₃ nanoparticles against Gram-positive and Gram-negative bacteria by disc diffusion method. The size of the zone of inhibition formed around each well of bacteria indicating the activity of Fe₂O₃ nanoparticles (a) *S. aureus* (b) *E. coli* (c) *K. pneumoniae* where (B-control, 1–10 µg/mL, 2–20 µg/mL, 3–30 µg/mL and 4–40 µg/mL).

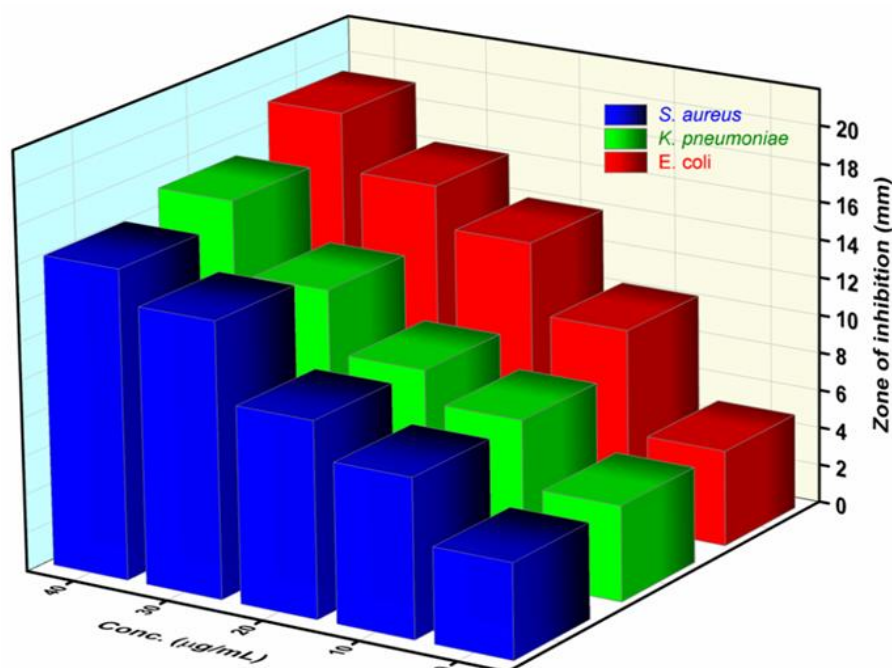


Figure 8. 3D representation of the inhibition zone formed around respective discs of bacteria *S. aureus*, *K. pneumoniae*, and *E. coli* representing the activity of Fe₂O₃ nanoparticles.

Table 1. Antibacterial activity of synthesized Fe₂O₃ nanoparticles against the pathogen (* including disc size).

Concentration (µg/mL)	* Zone of Inhibition (mm) Mean ± SD		
	<i>S. aureus</i>	<i>K. pneumoniae</i>	<i>E. coli</i>
Control	5	5	5
10	8.3 ± 0.4	8.4 ± 0.4	10.4 ± 0.5
20	10.2 ± 0.2	10.1 ± 0.1	14.1 ± 0.1
30	14.4 ± 0.3	13.4 ± 0.4	16.3 ± 0.3
40	16.2 ± 0.2	17.2 ± 0.2	19.3 ± 0.3

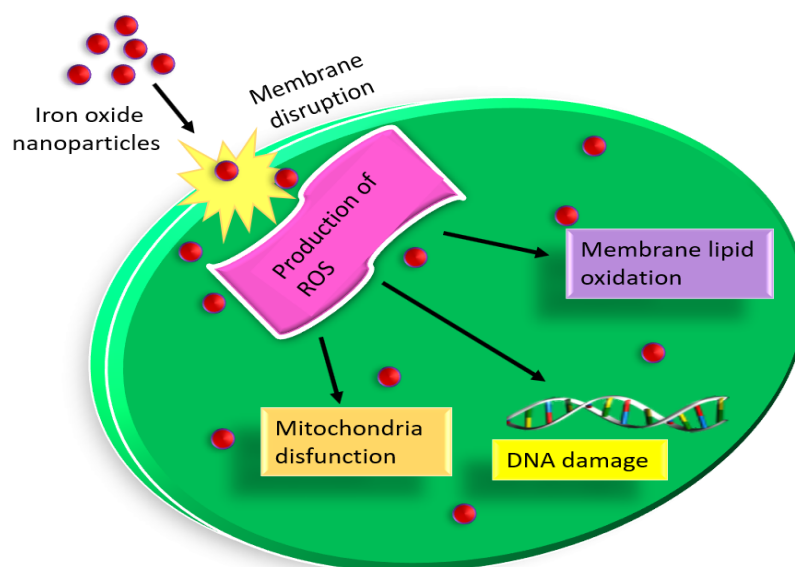


Figure 9. Schematic representation for a possible mechanism of Fe_2O_3 nanoparticles towards antibacterial activity. The effectiveness of Fe_2O_3 nanoparticles is based on the production of ROS, which is responsible for the cell death of microorganisms. ROS production cannot develop immunity because since ROS attack many different sites and biomolecules in the microorganism, they cannot develop resistance resulting in oxidation and cell death.

3.5. Antioxidant Efficiency of Fe_2O_3 Nanoparticles: A Possible Mechanism of Action for Antibacterial and Cytotoxic Activity

DPPH and nitric oxide (NO) scavenging assays were carried out to determine the antioxidant phenomenon of Fe_2O_3 nanoparticles (Figure 10). DPPH is a stable free radical delocalizing throughout the entire molecule to prevent its dimerization [55,56]. The DPPH was reduced to the formed stable, diamagnetic molecule when the nanoparticle was mixed with the solution resulting in changing the color of the solution from yellow to violet color. If the DPPH molecule is shown by $\text{X}\bullet$ and the donor molecule by ZH , the primary reaction is defined as $\text{X}\bullet + \text{ZH} = \text{XH} + \text{Z}^*$, where XH meant reduced form and Z^* meant free radical. According to the UV-vis absorption curve in Figure 10a, the antioxidant potential of Fe_2O_3 nanoparticles was dose-dependent. The potential for inhibition in the production of nitrite with oxygen and oxides carried out the NO scavenging activity (Figure 10b). The overall findings demonstrated that at a concentration of $800 \mu\text{g}/\text{mL}$, Fe_2O_3 nanoparticles exhibited high activity. The antibacterial and cell cytotoxic potential can be attributed to scavenging activity [57].

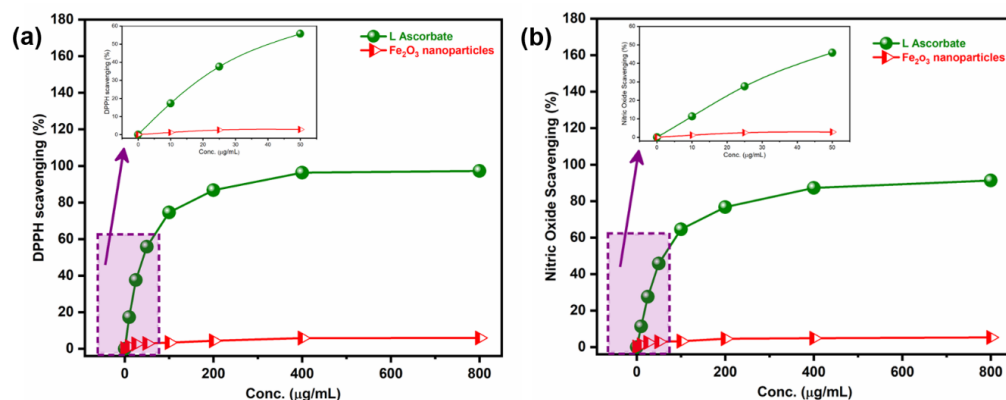


Figure 10. Antioxidant activity of Fe_2O_3 nanoparticles. (a) DPPH radical scavenging assay. (b) Nitric oxide scavenging assay showing the potential of synthesized Fe_2O_3 nanoparticles.

4. Conclusions

Since physiological processes occur at the nanoscale, many biological and medical issues are anticipated to be resolved through the use of nanotechnology and nanoparticles. To understand the mode of action and impact of various coatings to counteract the negative effect at the cellular level and optimize the potential of our nanoparticles for nanomedicine, a tailored investigation against each aspect is required. Our research revealed that Fe₂O₃ nanoparticle exposure to MCF-7 cells causes considerable cytotoxicity, opening up new possibilities for the safe delivery of Fe₂O₃ nanoparticles and their use in anticancer therapies. Additionally, it demonstrated another role in bacteria's antimicrobial ability. Moreover, further research on the toxicity and biocompatibility aspects of animal models is also recommended to further understand their safety and biocompatible nature. Therefore, we may conclude that Fe₂O₃ nanoparticles can be employed as an acceptable substitute for an antibacterial drug that received clinical approval.

Author Contributions: Conceptualization, N.T. and M.P.S.; methodology, N.T. and V.S.; software, N.T.; validation, N.T. and V.S.; formal analysis, N.T.; investigation, N.T.; data curation, N.T. and V.S.; writing—original draft preparation, N.T. and M.P.S.; writing—review and editing, N.T., V.K.C., M.P.S., and E.V.; visualization, N.T. and M.P.S.; supervision, M.P.S. All authors have read and agreed to the published version of the manuscript.

Funding: The authors declare that no funds, grants, or other support were received during the preparation of this manuscript.

Institutional Review Board Statement: Not applicable.

Informed Consent Statement: Not applicable.

Data Availability Statement: All data relevant to the publication are included.

Acknowledgments: N.T. gratefully acknowledges the University Grants Commission (UGC), New Delhi, for providing fellowship to pursue a Ph.D. All the authors also acknowledge the Central Research Facility (CRF), IIT Delhi and Centre for Interdisciplinary Research (CIR), MNNIT, Allahabad.

Conflicts of Interest: The authors declare no conflict of interest.

References

1. Khan, I.; Saeed, K.; Khan, I. Nanoparticles: Properties, applications and toxicities. *Arab. J. Chem.* **2019**, *12*, 908–931. [[CrossRef](#)]
2. Salata, O.V. Applications of nanoparticles in biology and medicine. *J. Nanobiotechnol.* **2004**, *2*, 3. [[CrossRef](#)] [[PubMed](#)]
3. Soni, A.; Bhandari, M.P.; Tripathi, G.K.; Bundela, P.; Khiriya, P.K.; Khare, P.S.; Pérez de la Lastra, J.M. Nano-biotechnology in tumour and cancerous disease: A perspective review. *J. Cell. Mol. Med.* **2023**, *27*, 737–762. [[CrossRef](#)] [[PubMed](#)]
4. Dutt, Y.; Pandey, R.P.; Dutt, M.; Gupta, A.; Vibhuti, A.; Vidic, J.; Priyadarshini, A. Therapeutic applications of nanobiotechnology. *J. Nanobiotech.* **2023**, *21*, 148. [[CrossRef](#)] [[PubMed](#)]
5. Ullah, Z.; Gul, F.; Iqbal, J.; Abbasi, B.A.; Kanwal, S.; Chalgham, W.; El-Sheikh, M.A.; Diltemiz, S.A.; Mahmood, T. Biogenic Synthesis of Multifunctional Silver Oxide Nanoparticles (Ag₂ONPs) Using *Parietaria alsinaefolia* Delile Aqueous Extract and Assessment of Their Diverse Biological Applications. *Microorganisms* **2023**, *11*, 1069. [[CrossRef](#)]
6. Malik, S.B.; Gul, A.; Saggu, J.I.; Abbasi, B.A.; Azad, B.; Iqbal, J.; Kazi, M.; Chalgham, W.; Firoozabadi, S.A.M. Fabrication and Characterization of Ag-Graphene Nanocomposites and Investigation of Their Cytotoxic, Antifungal and Photocatalytic Potential. *Molecules* **2023**, *28*, 4139. [[CrossRef](#)]
7. Haris, M.; Fatima, N.; Iqbal, J.; Chalgham, W.; Mumtaz, A.S.; El-Sheikh, M.A.; Tavafoghi, M. Oscillatoria limnetica Mediated Green Synthesis of Iron Oxide (Fe₂O₃) Nanoparticles and Their Diverse In Vitro Bioactivities. *Molecules* **2023**, *28*, 2091. [[CrossRef](#)]
8. Zhang, Q.; Yang, X.; Guan, J. Applications of magnetic nanomaterials in heterogeneous catalysis. *ACS Appl. Nano Mater.* **2019**, *2*, 4681–4697. [[CrossRef](#)]
9. Nandwana, V.; De, M.; Chu, S.; Jaiswal, M.; Rotz, M.; Meade, T.J.; Dravid, V.P. Theranostic magnetic nanostructures (MNS) for cancer. *Cancer Treat. Res.* **2015**, *166*, 51–83. [[CrossRef](#)]
10. Zhao, S.; Yu, X.; Qian, Y.; Chen, W.; Shen, J. Multifunctional magnetic iron oxide nanoparticles: An advanced platform for cancer theranostics. *Theranostics* **2020**, *10*, 6278. Available online: <https://www.thno.org/v10p6278.html> (accessed on 15 May 2020). [[CrossRef](#)]
11. Cui, H.; Liu, Y.; Ren, W. Structure switch between α -Fe₂O₃, γ -Fe₂O₃ and Fe₃O₄ during the large scale and low temperature sol-gel synthesis of nearly monodispersed iron oxide nanoparticles. *Adv. Powder Technol.* **2013**, *24*, 93–97. [[CrossRef](#)]

12. Wu, W.; Wu, Z.; Yu, T.; Jiang, C.; Kim, W.S. Recent progress on magnetic iron oxide nanoparticles: Synthesis, surface functional strategies and biomedical applications. *Sci. Technol. Adv. Mater.* **2015**, *16*, 023501. [[CrossRef](#)] [[PubMed](#)]
13. Ajinkya, N.; Yu, X.; Kaithal, P.; Luo, H.; Somani, P.; Ramakrishna, S. Magnetic Iron Oxide Nanoparticle (IONP) Synthesis to Applications: Present and Future. *Materials* **2020**, *13*, 4644. [[CrossRef](#)] [[PubMed](#)]
14. Tadic, M.; Panjan, M.; Damjanovic, V.; Milosevic, I. Magnetic properties of hematite (α -Fe₂O₃) nanoparticles prepared by hydrothermal synthesis method. *Appl. Surf. Sci.* **2014**, *320*, 183–187. [[CrossRef](#)]
15. Vecchio, C.L.; Trocino, S.; Zignani, S.C.; Baglio, V.; Carbone, A.; Garcia, M.I.D.; Aricò, A.S. Enhanced photoelectrochemical water splitting at hematite photoanodes by effect of a NiFe-oxide co-catalyst. *Catalysts* **2020**, *10*, 525. [[CrossRef](#)]
16. Arias, L.S.; Pessan, J.P.; Vieira, A.P.M.; Lima, T.M.T.D.; Delbem, A.C.B.; Monteiro, D.R. Iron oxide nanoparticles for biomedical applications: A perspective on synthesis, drugs, antimicrobial activity, and toxicity. *Antibiotics* **2018**, *7*, 46. [[CrossRef](#)]
17. Besenhard, M.O.; LaGrow, A.P.; Hodzic, A.; Kriechbaum, M.; Panariello, L.; Bais, G.; Gavrilidis, A. Co-precipitation synthesis of stable iron oxide nanoparticles with NaOH: New insights and continuous production via flow chemistry. *Chem. Eng. Process.* **2020**, *399*, 125740. [[CrossRef](#)]
18. Arsalani, S.; Oliveira, J.; Guidelli, E.J.; Araujo, J.F.; Wiekhorst, F.; Baffa, O. Synthesis of radioluminescent iron oxide nanoparticles functionalized by anthracene for biomedical applications. *Colloids Surf. A Physicochem. Eng. Asp.* **2020**, *602*, 125105. [[CrossRef](#)]
19. Saqib, S.; Munis, M.F.H.; Zaman, W.; Ullah, F.; Shah, S.N.; Ayaz, A.; Bahadur, S. Synthesis, characterization and use of iron oxide nano particles for antibacterial activity. *Microsc. Res. Tech.* **2019**, *82*, 415–420. [[CrossRef](#)]
20. Farahmandjou, M.; Soflaee, F. Synthesis and characterization of α -Fe₂O₃ nanoparticles by simple co-precipitation method. *Phys. Chem. Res.* **2015**, *3*, 191–196. [[CrossRef](#)]
21. Ali, A.; Hira Zafar, M.Z.; ul Haq, I.; Phull, A.R.; Ali, J.S.; Hussain, A. Synthesis, characterization, applications, and challenges of iron oxide nanoparticles. *Nanotech. Sci. Appl.* **2016**, *9*, 49. [[CrossRef](#)] [[PubMed](#)]
22. Alangari, A.; Alqahtani, M.S.; Mateen, A.; Kalam, M.A.; Alshememry, A.; Ali, R.; Syed, R. Iron oxide nanoparticles: Preparation, characterization, and assessment of antimicrobial and anticancer activity. *Adsorp. Sci. Technol.* **2022**, *2022*, 1562051. [[CrossRef](#)]
23. Pradhan, D.; Pradhan, S.; Behera, B.; Samantaray, A. Screening of Cytotoxic Activity of Hematite (α -Fe₂O₃) Nanoparticles from *Butea monosperma* on MCF-7 Cells. *Pharmacogn. Res.* **2021**, *13*, 260–266.
24. Ali, H.R.; Nassar, H.N.; El-Gendy, N.S. Green synthesis of α -Fe₂O₃ using Citrus reticulum peels extract and water decontamination from different organic pollutants. *Energy Sources Part A Recovery Util.* **2017**, *39*, 1425–1434. [[CrossRef](#)]
25. Mosdam, T. Rapid colorimetric assay for cellular growth and survival: Application to proliferation and cytotoxic assay. *J. Immunol. Methods* **1983**, *65*, 55–63. [[CrossRef](#)]
26. Kasithevar, M.; Saravanan, M.; Prakash, P.; Kumar, H.; Ovais, M.; Barabadi, H.; Shinwari, Z.K. Green synthesis of silver nanoparticles using *Alysicarpus monilifer* leaf extract and its antibacterial activity against MRSA and CoNS isolates in HIV patients. *J. Interdiscip. Nanomed.* **2017**, *2*, 131–141. [[CrossRef](#)]
27. Kurechi, T.; Kikugawa, K.; Kato, T. Studies on the antioxidants. XIII. Hydrogen donating capability of antioxidants to 2, 2-diphenyl-1-picrylhydrazyl. *Chem. Pharm. Bull.* **1980**, *28*, 2089–2093. [[CrossRef](#)]
28. Pourmadadi, M.; Rahmani, E.; Shamsabadipour, A.; Mahtabian, S.; Ahmadi, M.; Rahdar, A.; Díez-Pascual, A.M. Role of Iron Oxide (Fe₂O₃) Nanocomposites in Advanced Biomedical Applications: A State-of-the-Art Review. *Nanomaterials* **2022**, *12*, 3873. [[CrossRef](#)]
29. Xu, Y.Y.; Zhao, D.; Zhang, X.J.; Jin, W.T.; Kashkarov, P.; Zhang, H. Synthesis and characterization of single-crystalline α -Fe₂O₃ nanoleaves. *Phys. E Low. Dimens. Syst. Nanostruct.* **2009**, *41*, 806–811. [[CrossRef](#)]
30. Zhang, G.Y.; Xu, Y.Y.; Gao, D.Z.; Sun, Y.Q. α -Fe₂O₃ nanoplates: PEG-600 assisted hydrothermal synthesis and formation mechanism. *J. Alloys Compd.* **2011**, *509*, 885–890. [[CrossRef](#)]
31. Zotti, G.; Schiavon, G.; Zecchin, S.; Casellato, U. Electrodeposition of Amorphous Fe₂O₃ Films by Reduction of Iron Perchlorate in Acetonitrile. *J. Electrochem. Soc.* **1998**, *145*, 385. [[CrossRef](#)]
32. Beermann, N.; Vayssieres, L.; Lindquist, S.E.; Hagfeldt, A. (Photoelectrochemical studies of oriented nanorod thin films of hematite. *J. Electrochem. Soc.* **2000**, *147*, 2456. [[CrossRef](#)]
33. Vayssieres, L.; Sathe, C.; Butorin, S.M.; Shuh, D.K.; Nordgren, J.; Guo, J. One-dimensional quantum-confinement effect in α -Fe₂O₃ ultrafine nanorod arrays. *Advanc. Mater.* **2005**, *17*, 2320–2323. [[CrossRef](#)]
34. Goyal, R.N.; Pandey, A.K.; Kaur, D.; Kumar, A. Fabrication of α -Fe₂O₃ nanopowder modified glassy carbon electrode for applications in electrochemical sensing. *J. Nanosci. Nanotechnol.* **2009**, *9*, 4692–4699. [[CrossRef](#)]
35. Sivakumar, S.; Anusuya, D.; Khatiwada, C.P.; Sivasubramanian, J.; Venkatesan, A.; Soundhirarajan, P. Characterizations of diverse mole of pure and Ni-doped α -Fe₂O₃ synthesized nanoparticles through chemical precipitation route. *Spectrochim. Acta A Mol. Biomol. Spectrosc.* **2014**, *128*, 69–75. [[CrossRef](#)] [[PubMed](#)]
36. Patterson, A.L. The Scherrer formula for X-ray particle size determination. *Phys. Rev.* **1939**, *56*, 978. [[CrossRef](#)]
37. Darezereshki, E. One-step synthesis of hematite (α -Fe₂O₃) nano-particles by direct thermal-decomposition of maghemite. *Mater. Lett.* **2011**, *65*, 642–645. [[CrossRef](#)]
38. Pal, B.; Sharon, M. Preparation of iron oxide thin film by metal organic deposition from Fe (III)-acetylacetonate: A study of photocatalytic properties. *Thin Solid Film.* **2000**, *379*, 83–88. [[CrossRef](#)]
39. Parhizkar, J.; Habibi, M.H. Synthesis, characterization and photocatalytic properties of Iron oxide nanoparticles synthesized by sol-gel autocombustion with ultrasonic irradiation. *Nanochem. Res.* **2017**, *2*, 166–171. [[CrossRef](#)]

40. Jafarirad, S.; Hammami Torghabe, E.; Rasta, S.H.; Salehi, R. A novel non-invasive strategy for low-level laser-induced cancer therapy by using new Ag/ZnO and Nd/ZnO functionalized reduced graphene oxide nanocomposites. *Artif. Cells Nanomed. Biotechnol.* **2018**, *46*, 800–816. [[CrossRef](#)] [[PubMed](#)]
41. Lee, B.; Lee, D.G. Synergistic antibacterial activity of gold nanoparticles caused by apoptosis-like death. *J. Appl. Microbiol.* **2019**, *127*, 701–712. [[CrossRef](#)]
42. Wang, Y.; Chinnathambi, A.; Nasif, O.; Alharbi, S.A. Green synthesis and chemical characterization of a novel anti-human pancreatic cancer supplement by silver nanoparticles containing Zingiber officinale leaf aqueous extract. *Arab. J. Chem.* **2021**, *14*, 103081. [[CrossRef](#)]
43. Bhushan, M.; Kumar, Y.; Periyasamy, L.; Viswanath, A.K. Antibacterial applications of α -Fe₂O₃/Co₃O₄ nanocomposites and study of their structural, optical, magnetic and cytotoxic characteristics. *Appl. Nanosci.* **2018**, *8*, 137–153. [[CrossRef](#)]
44. Das, S.; Diyali, S.; Vinothini, G.; Perumalsamy, B.; Balakrishnan, G.; Ramasamy, T.; Biswas, B. Synthesis, morphological analysis, antibacterial activity of iron oxide nanoparticles and the cytotoxic effect on lung cancer cell line. *Heliyon* **2020**, *6*, 04953. [[CrossRef](#)] [[PubMed](#)]
45. Henle, E.S.; Linn, S. Formation, prevention, and repair of DNA damage by iron/hydrogen peroxide. *J. Biol. Chem.* **1997**, *272*, 19095–19098. [[CrossRef](#)]
46. Armijo, L.M.; Wawrzyniec, S.J.; Kopciuch, M.; Brandt, Y.I.; Rivera, A.C.; Withers, N.J.; Osiński, M. Antibacterial activity of iron oxide, iron nitride, and tobramycin conjugated nanoparticles against Pseudomonas aeruginosa biofilms. *J. Nanobiotech.* **2020**, *18*, 35. [[CrossRef](#)]
47. Behera, S.S.; Patra, J.K.; Pramanik, K.; Panda, N.; Thatoi, H. Characterization and evaluation of antibacterial activities of chemically synthesized iron oxide nanoparticles. *World J. Nano. Sci. Eng.* **2012**, *2*, 196–200. [[CrossRef](#)]
48. Hancock, J.T.; Desikan, R.; Neill, S.J. Role of reactive oxygen species in cell signalling pathways. *Biochem. Soc. Trans.* **2001**, *29*, 345–349. [[CrossRef](#)]
49. Park, H.J.; Kim, J.Y.; Kim, J.; Lee, J.H.; Hahn, J.S.; Gu, M.B.; Yoon, J. Silver-ion-mediated reactive oxygen species generation affecting bactericidal activity. *Water Res.* **2009**, *43*, 1027–1032. [[CrossRef](#)] [[PubMed](#)]
50. Keenan, C.R.; Sedlak, D.L. Factors affecting the yield of oxidants from the reaction of nanoparticulate zero-valent iron and oxygen. *Environ. Sci. Technol.* **2008**, *42*, 1262–1267. [[CrossRef](#)] [[PubMed](#)]
51. Vasantharaj, S.; Sathiyavimal, S.; Senthilkumar, P.; LewisOscar, F.; Pugazhendhi, A. Biosynthesis of iron oxide nanoparticles using leaf extract of Ruellia tuberosa: Antimicrobial properties and their applications in photocatalytic degradation. *J. Photochem. Photobiol. B Biol.* **2019**, *192*, 74–82. [[CrossRef](#)] [[PubMed](#)]
52. Singh, M.P.; Rai, S.N.; Dubey, S.K.; Pandey, A.T.; Tabassum, N.; Chaturvedi, V.K.; Singh, N.B. Biomolecules of mushroom: A recipe of human wellness. *Crit. Rev. Biotechnol.* **2022**, *42*, 913–930. [[CrossRef](#)]
53. Kim, J.S.; Kuk, E.; Yu, K.N.; Kim, J.H.; Park, S.J.; Lee, H.J.; Cho, M.H. Antimicrobial effects of silver nanoparticles. *Nanomed. Nanotechnol. Biol. Med.* **2007**, *3*, 95–101. [[CrossRef](#)] [[PubMed](#)]
54. Tabassum, N.; Kumar, D.; Verma, D.; Bohara, R.A.; Singh, M.P. Zirconium oxide (ZrO₂) nanoparticles from antibacterial activity to cytotoxicity: A next-generation of multifunctional nanoparticles. *Mater. Today Commun.* **2021**, *26*, 102156. [[CrossRef](#)]
55. Bhakya, S.; Muthukrishnan, S.; Sukumaran, M.; Muthukumar, M. Biogenic synthesis of silver nanoparticles and their antioxidant and antibacterial activity. *Appl. Nanosci.* **2016**, *6*, 755–766. [[CrossRef](#)]
56. Contreras-Guzmán, E.S.; Strong, F.C. Determination of tocopherols (vitamin E) by reduction of cupric ion. *J. Assoc. Off. Anal. Chem.* **1982**, *65*, 1215–1221. [[CrossRef](#)]
57. Catana, R.; Helepciuc, F.E.; Zamfir, M.; Florescu, L.; Mitoi, M. In vivo and in vitro antioxidant activity of *Cnicus benedictus*. *AgroLife Sci. J.* **2020**, *9*, 73–78.

Disclaimer/Publisher’s Note: The statements, opinions and data contained in all publications are solely those of the individual author(s) and contributor(s) and not of MDPI and/or the editor(s). MDPI and/or the editor(s) disclaim responsibility for any injury to people or property resulting from any ideas, methods, instructions or products referred to in the content.